Combustion and Flame 178 (2017) 70–81

Contents lists available at ScienceDirect

Combustion and Flame

journal homepage: www.elsevier.com/locate/combustflame

Turbulence effects on the autoignition of DME in a turbulent co-flowing jet

Tarek Echekki [a,*], Samer F. Ahmed [b]

[a] Department of Mechanical and Aerospace Engineering, Campus Box 7910, North Carolina State University, Raleigh 27695, NC, USA
[b] Thermofluids Group, Department of Mechanical and Industrial Engineering, College of Engineering, Qatar University, P.O. Box 2713, Doha, Qatar

ARTICLE INFO

Article history:
Received 1 September 2016
Revised 12 October 2016
Accepted 20 December 2016
Available online 5 February 2017

Keywords:
Turbulent jet ignition
The one-dimensional turbulence model
Autoignition
DME fuel

ABSTRACT

Dimethyl ether (DME) autoignition in turbulent co-flowing jets with preheated air is studied using the one-dimensional turbulence (ODT) model. We investigate the effects of molecular and turbulent transport on the autoignition process at different jet Reynolds numbers and two air preheat conditions. Statistics for the cases considered show that the overall effects of turbulence and molecular transport can serve to delay or accelerate autoignition depending upon where ignition starts, the presence of 2-stage or single-stage ignition and the variations in ignition delay times in mixture fraction space. For the higher temperature air preheat cases, the classical view that autoignition is delayed by turbulence is established. For the lower preheat air temperature cases, we show that low-temperature chemistry associated with first-stage ignition can help accelerate the autoignition process and the transition to high-temperature chemistry. This acceleration can reduce the ignition delay time by as much as a factor of 2. Given this work and previous work by the authors based on a different fuel, n-heptane, we find that the ignition delay map based on homogeneous ignition for different mixture fractions can provide a preview of the ignition scenarios for the co-flowing jet configuration regardless of the choice of fuel considered.

1. Introduction

Many practical combustion fuels exhibit multi-stage ignition associated with the so-called negative temperature coefficient (NTC) behavior. This behavior introduces additional key chemical time scales associated with the different stages of ignition. This behavior is critical for a broad range of practical fuels; yet, we are only beginning to understand various scenarios where NTC behavior coupled with chemistry can exhibit unexpected results. It has been commonly assumed that turbulence serves to delay ignition because of the inherent role of dissipation in depleting nascent flame kernels of key radicals and heat [1–8]. However, recent studies suggest that the coupling of reaction and transport (turbulent or molecular) can yield complex interactions that may or may not fall into the common view of the role of turbulent transport (see for example, [9–14]).

In a recent study, the authors investigated the coupling of chemistry and transport in a jet configuration of n-heptane, a fuel subject to NTC behavior, in preheated co-flow air at various jet Reynolds numbers [14] using the one-dimensional turbulence (ODT) model [15]. We have observed a mechanism by which turbulent and molecular transport can accelerate the autoignition process through transport from layers in the fluid experiencing first-stage ignition to layers evolving eventually to their second- or final-stage ignition. However, this mechanism is only one possible scenario where transport can potentially accelerate ignition under turbulence conditions. More importantly, ignition delay maps relating ignition delay for first and second stage ignitions vs. mixture fraction based on homogeneous ignition helped explain the trends exhibited in the jet simulations.

The coupling of first-stage and second-stage chemistries has been identified by other authors within the context of non-premixed flame stabilization [16–19] and related to the fuel being considered in this study, which is dimethyl ether (DME). For example, Deng et al. [16] showed that at an intermediate temperature range for the co-flow air in a stabilized non-premixed DME/air jet flame, NTC chemistry determines the stabilization point in mixture fraction space. Minomoto and Chen [19] also show that the propagation speed at the triple point of a stabilized DME/air slot jet flame is also influenced by two-stage ignition.

The objective of this study is to explore and identify additional scenarios exhibited by fuels subject to NTC behavior under turbulence conditions. More importantly, we attempt to preview such scenarios using ignition delay maps based on homogeneous ignition calculations. The study is based on the ODT

* Corresponding author.
E-mail address: techekk@ncsu.edu (T. Echekki).

http://dx.doi.org/10.1016/j.combustflame.2016.12.022
0010-2180/

model applied to DME, a relatively simple fuel to heavier hydrocarbons that exhibits NTC behavior, in a co-flowing jet configuration. To overcome potential limitations of reduced mechanisms for complex fuels, which are validated for simple reactor models, we will use the detailed mechanism proposed by Zhao et al. [20]. This mechanism captures both low-temperature and high-temperature kinetics for DME. There are several detailed mechanisms for DME, which are available in the literature [21–26]. The mechanism by Zhao et al. [20] has been validated against a host of experiments spanning the low- and high-temperature regimes in combustion, including experiments based on flow reactors, shock tubes, jet-stirred reactors and burner-stabilized premixed flames [20]. In the present study, to further characterize the NTC behavior, we also carry out 0D simulations.

2. Model formulations and run conditions

Two types of simulations are implemented, which include: 1) zero-dimensional homogeneous reaction ignition, and 2) one-dimensional stochastic model that emulates combustion in a jet configuration. The two models are described below.

2.1. 0D simulations

The zero-dimensional simulations serve as references for autoignition studies in the presence of turbulence and molecular transport. The governing equations for a zero-dimensional constant pressure system comprised of N chemical species correspond to the species and the temperature equations:

- The species equation:

$$\frac{\partial Y_k}{\partial t} = \frac{\dot{\omega}_k}{\rho}. \tag{1}$$

- The temperature equation:

$$\frac{\partial T}{\partial t} = -\frac{1}{\rho \bar{c}_p} \sum_{k=1}^{N} h_k \dot{\omega}_k. \tag{2}$$

In the above equations, t is the independent variable, which corresponds to time; T is the temperature; Y_k is the kth species mass fraction; ρ is the mixture density; $\dot{\omega}_k$ is the kth species reaction rates; $\bar{c}_p$ is the mixture specific heat; and h_k is the kth species total enthalpy. The thermodynamic pressure, p, is assumed to be constant, and the equation of state:

$$\rho = \frac{p}{R_u T \sum_{k=1}^{N} (Y_k/W_k)}, \tag{3}$$

can be used to determine the mixture density. The governing equations are integrated using a modified version of the CHEMKIN II code SENKIN [27].

The solution usually starts with an initial homogeneous mixture of fuel and oxidizer at different equivalence ratios from lean to rich. By varying the mixture fraction, different fuel and preheated oxidizer compositions are obtained. These initial compositions of the mixture based on the prescribed mixture fraction, Z, are prescribed as follows:

$$Y_{\text{Fuel}} = Z, \; Y_{\text{Oxidizer}} = 1 - Z. \tag{4}$$

The corresponding mixture temperature, T_{mix}, is evaluated by adiabatic mixing of the preheated air with the fuel at the prescribed mixture fraction:

$$\begin{aligned} &Z \times h_{\text{Fuel}}(T_{\text{Fuel}}) + (1-Z) \times h_{\text{Oxidizer}}(T_{\text{Oxidizer}}) \\ &\quad = Z \times h_{\text{Fuel}}(T_{\text{mix}}) + (1-Z) \times h_{\text{Oxidizer}}(T_{\text{mix}}) \end{aligned} \tag{5}$$

The scope of the homogeneous ignition study is to identify the various ignition scenarios at different mixture fractions and to provide a reference case for comparison with jet autoignition.

2.2. ODT simulations

A detailed description of the ODT model formulation for the jet configuration is given by Echekki et al. [15]. The ODT model is based on a deterministic implementation of reaction and diffusion and a stochastic implementation of turbulent advection in a space- and time-resolved simulation on a 1D domain. In this problem, the 1D domain corresponds to the transverse direction of the mean flow. Therefore, the formulation is based on a planar temporally-developing jet configuration. The formulation is built on the two key assumptions: (1) a parabolic flow formulation where transverse processes are dominant and streamwise downstream processes are less important, and (2) the time scales governed by the shear (in the transverse direction) are representative of the time scales representing stirring process in the jet. Moreover, as indicated in Echekki et al. [15], there are inherently similar scaling relations for the velocity decay between a planar temporally-developing jet (as implemented here) and the spatially-developing round jet.

Molecular processes are prescribed by the following unsteady reaction-diffusion equations:

- The streamwise momentum equation:

$$\frac{\partial u}{\partial t} = \frac{1}{\rho} \frac{\partial}{\partial y} \left(\mu \frac{\partial u}{\partial y} \right). \tag{6}$$

- The species equation:

$$\frac{\partial Y_k}{\partial t} = -\frac{1}{\rho} \frac{\partial}{\partial y} (\rho V_k Y_k) + \frac{\dot{\omega}_k}{\rho}. \tag{7}$$

- The temperature equation:

$$\frac{\partial T}{\partial t} = \frac{1}{\rho \bar{c}_p} \sum_{k=1}^{N} c_{p,k} Y_k V_k \frac{\partial T}{\partial y} + \frac{1}{\rho \bar{c}_p} \frac{\partial}{\partial y} \left(\lambda \frac{\partial T}{\partial y} \right) - \frac{1}{\rho \bar{c}_p} \sum_{k=1}^{N} h_k \dot{\omega}_k. \tag{8}$$

The pressure is assumed to be spatially uniform and constant, and the equation of state (3) is used to determine the mixture mass density. $c_{p,k}$ and V_k represent the kth species specific heat and diffusion velocity, respectively; λ is the mixture thermal conductivity. Eqs. (6)–(8) represent a temporal solution of a turbulent jet flame. The temporal evolution may be interpreted, in a statistical sense, as a downstream spatial evolution (in x) of the 1D velocity and scalar profiles. However, this conversion is not implemented here and statistics are collected as a function of time to establish direct comparisons with the unsteady 0D simulations. Therefore, the simulations are implemented as temporal jet simulations for one principal reason: the progress in the autoignition process in a temporal jet can be compared directly to the homogeneous ignition results. Such comparisons, will enable an isolation of turbulent transport and molecular diffusion transport effects on the autoignition process. A direct conversion from temporal to spatial jet statistics can be carried out in principle by accounting for residence time effects associated with the different inlet velocities at the co-flowing streams.

In the jet simulations, turbulent advection is implemented stochastically using stirring events, each involving the application of a “triplet map” [15]. The frequency of stirring events is governed by the spatially-resolved evolving rate of shear in the jet. Two adjustable parameters, the so-called A and β [15], are identical to previous values used in jet configurations with ODT [14,28–32].

The initial configuration (also, corresponding to the jet inlet) consists of a 2D segregated central fuel jet of width 1.1 cm with preheated air in the co-flow. The spatial extent of the co-flow air depends primarily on the evolution of the jet and the Reynolds number resulting in computational domains of 16 cm to 24 cm

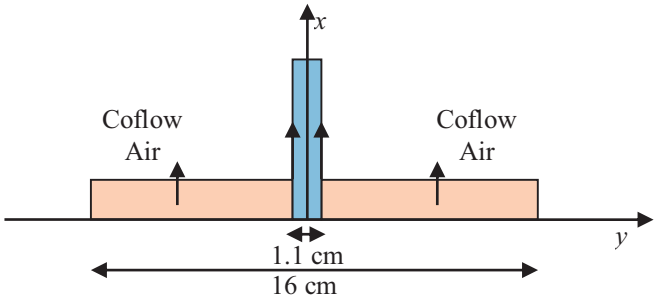

Fig. 1. Computational configuration and initial run condition. The extent of the computational domain of 16 cm in the transverse direction to the flow corresponds to a jet Reynolds number of 10,000.

with grid resolutions from 3200 to 4800 cells. Figure 1 shows the computational setup for the jet simulations along the *y*-direction. The top hat profiles for the velocities and fuel and oxidizer streams also correspond to the initial conditions for the ODT simulations.

The temporal discretization of the governing equations is based on full splitting of diffusion and reaction in which diffusion is advanced using the first-order Euler method, while the source term is integrated using a stiff-integrator, DVODE [33]. A second-order finite-difference scheme is used for spatial discretization. Transport properties for heat and mass are based on a mixture-averaged formulation and computed using transport libraries [34] within the Chemkin II suite [35]. The boundaries of the ODT are maintained at free-stream conditions throughout the jet.

The detailed mechanism of Zhao et al. [20] consists of 290 reversible reactions and 55 chemical species. Two sets of parametric studies were carried out. The first set corresponds to an oxidizer (air) preheat temperature of 750 K and the second corresponds to an oxidizer preheat temperature of 1200 K. Both studies use a fuel temperature of 300 K and a mixture at 1 atm. The choice of the studies is guided by the need to establish different scenarios for the autoignition process in the co-flowing jet configuration, which may be present in non-premixed and partially-premixed conditions under turbulence. It is important to note that, while we refer to the two preheat air studies as low and high-temperature conditions, this characterization is not a reflection of the type of chemistry, low- or high-temperature chemistries, involved. Indeed, both studies experience both types of chemistries, given the range of temperatures involved.

3. Results

3.1. Homogeneous ignition

The simulations are carried out using homogeneous chemistry calculations based on Eqs. (1) and (2) by varying the mixture fraction and, accordingly, the initial mixture temperature. Figure 2 shows the mixture temperature and the product (adiabatic flame) temperature as a function of the mixture fraction for both the lower and the higher temperature cases. Since the mixture is preheated on the oxidizer side, the slope of the mixture fraction is negative and is not linear, given the variations in the specific heats between fuel and oxidizer and their temperatures. The figure shows clearly that for a given mixture fraction, the corresponding mixture temperature is higher for the high-temperature case (the gap starts at 450 K at fuel-lean conditions and is zero at pure fuel). The stoichiometric mixture fraction for this mixture is 0.118. The figure shows that the products temperature for the low- and high-temperature cases peak at lean conditions (to the left of the stoichiometric value).

Figure 3 shows the evolution of the temperature in the mixture as a function of time for different values of the mixture fraction

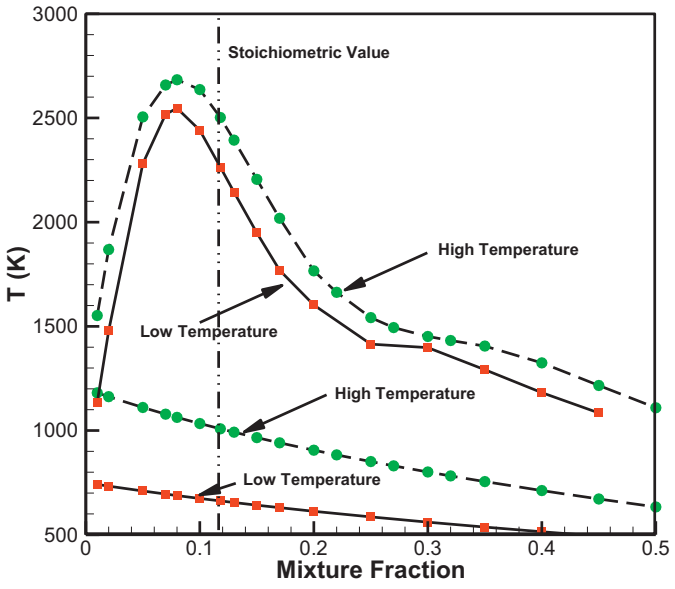

Fig. 2. Initial mixture temperature vs. mixture fraction for the low-temperature and the high-temperature computations.

for the low-temperature case. The figure shows that for the low-temperature conditions and for the mixture fractions shown, the ignition process is characterized by 2-stages with an initial small rise in temperature, followed by a much more pronounced rise corresponding to two-stage ignition. The gap between the two stages narrows as the mixture fraction is increased. In these cases, the first stage is delayed until it is merged with the second and final stage of ignition at higher mixture fractions.

A different trend is observed for the high-temperature cases as shown in Fig. 4. At these conditions, only single stage ignition is achieved for the mixture fractions shown in Fig. 3, $Z=0.118$, 0.15, 0.2 and 0.3. Two-stage ignition occurs for the higher-mixture fractions beyond $Z=0.3$ (as evidenced by the results discussed below).

Figure 5 shows the ignition delay times (first- and second-stages when applicable) for the low-temperature and the high-temperature simulations. Each data point indicated corresponds to a full chemistry homogeneous mixture simulation. The delay times are based on the peak of the temperature gradient, which is consistent with other measures, such as the peak of H mass fraction.

The low-temperature calculations show an important gap between the first-stage ignition delay and those of the second stage ignition times. This gap is largest at lower mixture fractions and it is narrower at higher mixture fractions. Eventually, these two times merge beyond the conditions shown. In contrast with the low-temperature cases, the high-temperature cases show a single-stage ignition from fuel-lean conditions to a value of Z near 0.3. Beyond this point, a gap is present between the 2 stages; but, this gap, too, closes at higher mixture fractions. As shown below, these differences play an important role when the role of (molecular or turbulent) transport is introduced in the turbulent jet configuration.

The profiles shown in Fig. 5 can be contrasted with the conditions considered in our recent work [14] with n-heptane autoignition based on two preheat conditions. There, Fig. 7 of Ref. [14] shows similar profiles for the low-temperature cases. However, for the higher temperature cases, the n-heptane autoignition delay data shows a decreasing first-stage ignition delay time as the mixture fraction is increased. We will revisit this difference between the higher temperature cases considered here and in Ref. [14] in Sections 3.2 and 4.

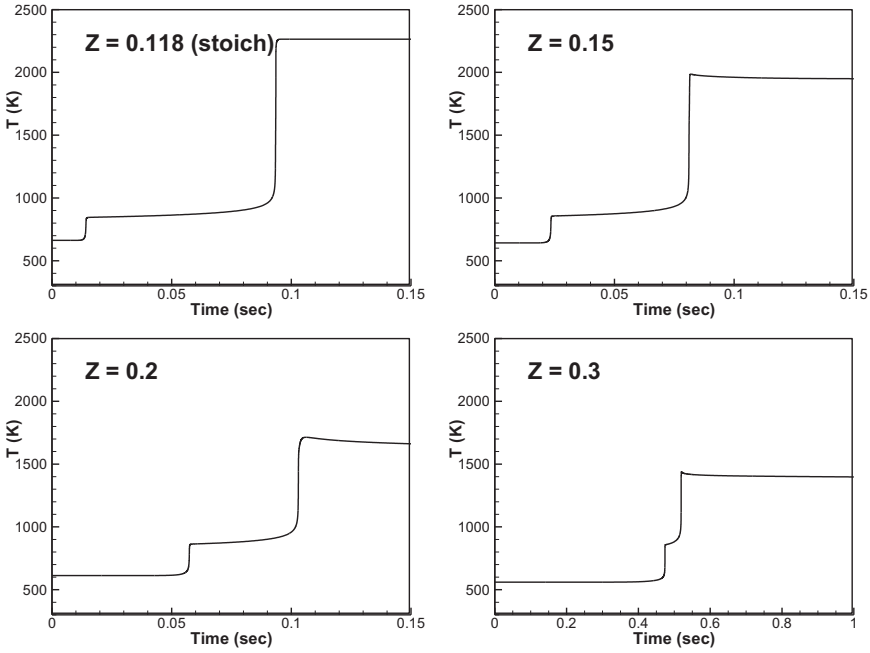

Fig. 3. Temperature evolution during ignition of the fuel air mixture at different mixture fractions at the low-temperature case.

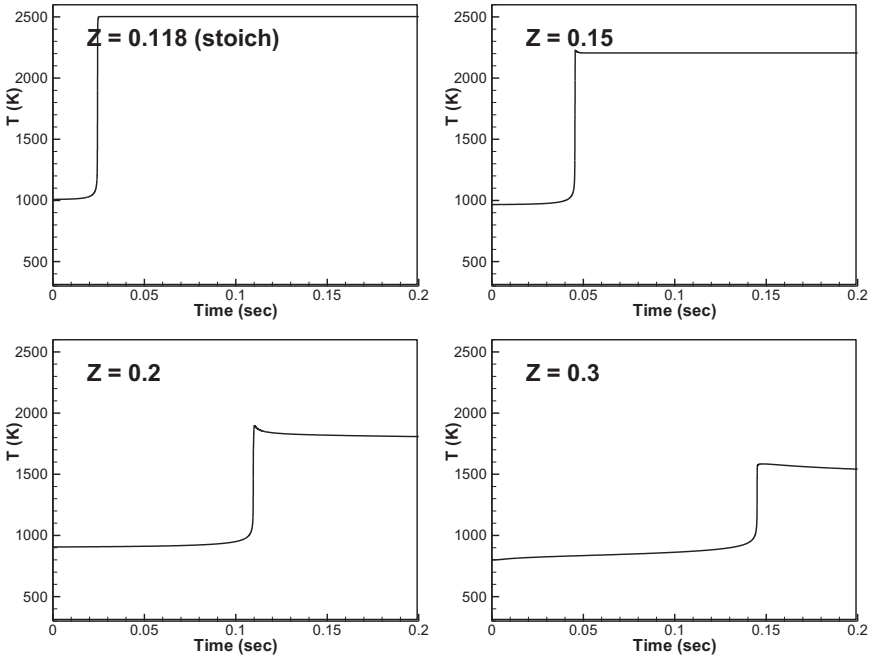

Fig. 4. Temperature evolution during ignition of the fuel air mixture at different mixture fractions at the high-temperature case.

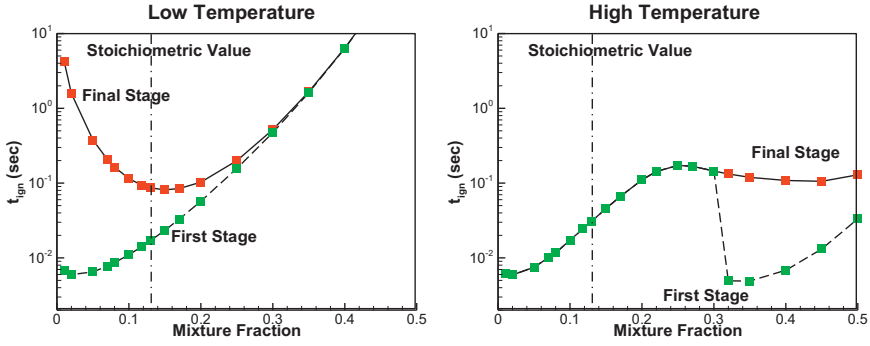

Fig. 5. Ignition delay times vs. mixture fraction for the low- and high- temperature computations.

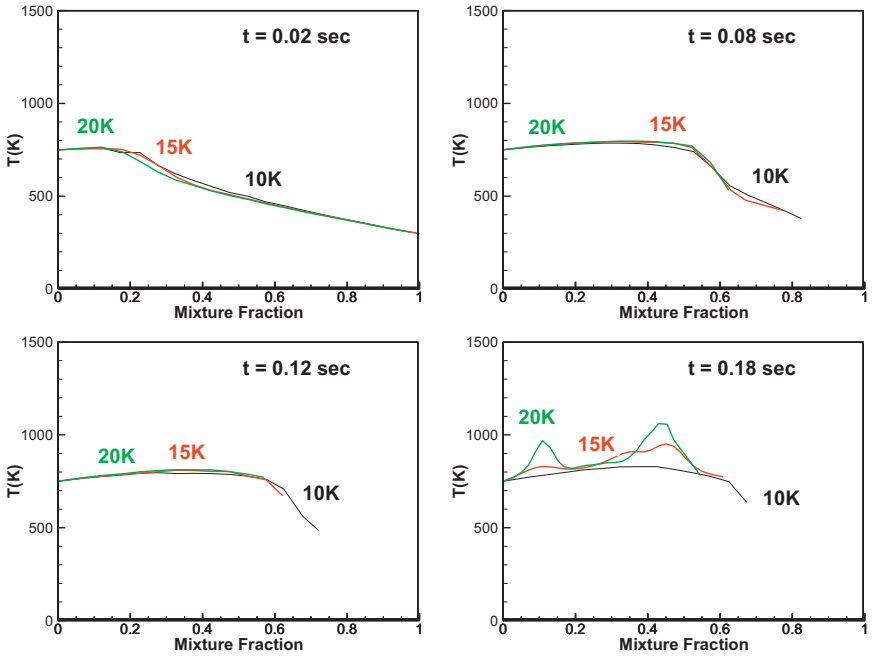

Fig. 6. Conditional means of temperature for Re = 10,000, 15,000 and 20,000 for the low-temperature conditions.

Table 1
Summary of run conditions. The fuel temperature is at 300 K and two co-flow air temperatures, 750 and 1200 K, are considered. The co-flow air velocity at the inlet is 100 cm/s. The fuel jet channel is 1.1 cm wide.

Reynolds number	Fuel jet velocity (cm/s)	Domain size (cm)	Computational cells
10,000	424.9	16	3200
15,000	637.4	20	4000
20,000	849.8	24	4800

3.2. Turbulent jet autoignition

The same cases of two different preheats of 750 K and 1200 K are considered in the turbulent jet autoignition studies. In these configurations, co-flowing streams of preheated air and fuel at 300 K are allowed to mix and react at different jet Reynolds numbers (based on the fuel inlet) of 10,000, 15,000 and 20,000. Table 1 summarizes the ODT run conditions corresponding to these jet Reynolds numbers.

The mechanisms governing autoignition under turbulent conditions between the low-temperature and the high-temperature cases can be investigated through statistics of key thermo-chemical scalars in mixture fraction space. Figures 6 and 7 show conditional means of temperature at Reynolds numbers of 10,000, 15,000 and 20,000 for the two cases considered, respectively, and at select times of the jet evolution. The statistics are based on 60 realizations for each Reynolds number and the two preheat cases; each realization takes 2–3 days to complete on a single Intel Xeon processor; although, optimization of the chemistry and transport modules in the code can potentially speed up the computations. The conditioning variable is the mixture fraction, which is expressed as [36]:

$$Z = \frac{2(Y_C - Y_{C,o})/W_C + (Y_H - Y_{H,o})/2W_H - (Y_O - Y_{O,o})/W_O}{2(Y_{C,f} - Y_{C,o})/W_C + (Y_{H,f} - Y_{H,o})/2W_H - (Y_{O,f} - Y_{O,o})/W_O} \quad (9)$$

where the Y's are the elemental mass fractions corresponding to C, H and O; the W's are atomic weights for C, H and O; and the subscripts f and o refer to the reference conditions of the fuel and the air, respectively. Comparisons of the different Reynolds numbers is a direct indication of the role of turbulence on the autoignition process.

Figure 6 shows that at 0.02 s, the temperature profile is very similar to that of the initial mixture temperature (see Fig. 2) and all Reynolds numbers exhibit initially similar magnitudes and shapes. At later times, 0.08 and 0.12 s, it is clear that the peak shifts towards richer conditions, while profiles remain flat from fuel-lean to a mixture fraction of approximately 0.6. In contrast to what is shown in Fig. 3, which indicates the onset of first-stage with a delay above 0.14 s for mixture fractions beyond 0.3, the conditional temperature means indicate higher temperatures as early as 0.08 s. This difference suggests an acceleration of the autoignition delay by approximately a factor of 2. This acceleration can be achieved primarily through either diffusive transport, turbulent transport or both, since both transport mechanisms are coupled. This transport transfers heat from first-stage ignition kernels at leaner mixtures (see Fig. 3) to rich mixtures. The higher Reynolds number case even shows that at 0.18 s, the final stage ignition is achieved (statistically) at mixture fractions slightly above 0.4. Further delay of this ignition occurs at later times for leaner mixtures. Therefore, turbulence, while initially contributing to a delay in the onset of first stage ignition, it has, clearly, accelerated the onset of the final stage ignition at fuel-rich conditions. A similar, yet non-monotonic, behavior as a function of jet Reynolds number is observed in the "low-temperature" conditions presented by the authors [14] for n-heptane as a fuel. Therefore, this observation further reinforces the potential scenario of the effect of first-stage ignition at a given mixture conditions on the acceleration of the final stage of ignition at adjacent mixtures.

It is equally important to note that at $t = 0.18$ s in Fig. 6, there are two peaks for the conditional mean of temperature. The peak at leaner mixtures corresponds approximately to the conditions of lowest second-stage ignition delay times in Fig. 5. Therefore, its transition to second-stage ignition is more likely attributed to a progress from first-stage ignition at the same mixture conditions.

A different scenario for the autoignition process is observed for the high-temperature case as shown in Fig. 7. In this case, turbulence is contributing to the delay in the autoignition

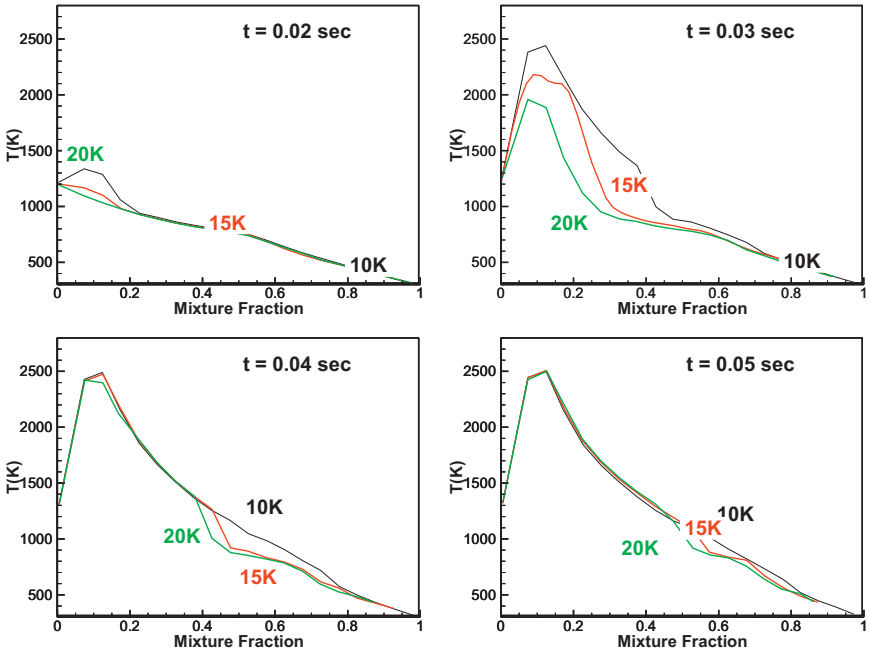

Fig. 7. Conditional means of temperature for Re = 10,000, 15,000 and 20,000 for the high-temperature conditions.

process throughout the mixture fraction space. Figure 7 shows that at 0.02 s, the temperature profile is very similar to that of the initial mixture temperature (see Fig. 2), except for the local peak near the stoichiometric condition. Based on the homogeneous ignition delay times, the timing of this peak can only correspond to a final stage ignition. This peak is more pronounced for the lower jet Reynolds number indicating that turbulence does contribute to a delay in the first stage of autoignition. The delayed ignition in this case is more pronounced at 0.03 s, where further lag is observed in the temperature profiles at a wide range of mixture conditions. At 0.04 and 0.05 s, there is a narrowing gap between 0.4 and 0.6 in mixture fraction space indicating further ignition delay at higher Reynolds numbers. This range also corresponds to a 2-stage ignition range in Fig. 5 where there is a discernable gap between the first and second-stage ignitions. The observation of the gap in the statistics has not been made for the "high-temperature" case in [14] for n-heptane flames. In the n-heptane scenario, the map of the ignition delay times as a function of temperature (Fig. 7 in [14]) exhibited a steady decrease in the first-stage ignition delay time as a function of mixture fraction. Therefore, the map of ignition delay time (Fig. 5 here and Fig. 7 in [14]) provides a preview of the outcome under molecular/turbulent transport conditions. Nonetheless, and despite this unique scenario exhibited by the present conditions, we find that at the high-temperature conditions considered, turbulence contributes to ignition delay.

A principal scope of our recent work has been to establish criteria to understand the role of turbulence and molecular mixing in the process of autoignition. To understand them, we have made additional comparisons based on the two preheat cases and the different Reynolds number cases. The comparisons are made based on two markers for low-temperature ignition and high-temperature ignition. The marker for high-temperature ignition is the hydroxyl radical OH (mass fraction and reaction); OH is produced during the two stages of ignition leading to heat release. However, OH peaks are much more pronounced during the second stage of ignition. The marker for low-temperature ignition is the intermediate species, methoxymethyl peroxy radical or $CH_3OCH_2O_2$. Krisman et al. [37] have found this radical to be an excellent indicator of low-temperature ignition.

Figure 8 compares profiles of OH (red) and $CH_3OCH_2O_2$ (black) mass fractions for the low-temperature case at different times. Note the different scales exhibited for different times. Both species peaks coincide at the same positions up to 0.12 s. The OH peaks may correspond to either first or second stage ignition, given that OH concentrations at the second stage ignition process at high mixture fractions also tend to be relatively low and comparable in magnitude to the near-stoichiometric mixture peaks at first-stage ignition. Much higher peaks for OH are exhibited at $t = 0.2$ s indicating clear conditions of second-stage ignition. The latter peaks occur at the edge of the high $CH_3OCH_2O_2$ mass fraction kernels. The figure shows that at 0.02 the peaks of $CH_3OCH_2O_2$ mass fraction are highest among the times shown indicating an early onset of first-stage ignition. The peaks of OH follow, consistently with 2-stage ignition.

Figure 9 compares profiles of OH (red) and $CH_3OCH_2O_2$ (black) mass fractions for the high-temperature case at different times. Again, note the variation of scales for the different times. The profiles show that, in contrast to the low-temperature case, both species peaks do not coincide at the same location. The OH peaks occur further away from the fuel jet, indicating conditions of lean mixtures; while, $CH_3OCH_2O_2$ peaks occur closer to the interface between the fuel and the oxidizer, indicating richer fuel conditions. Again, the peaks occur earlier for $CH_3OCH_2O_2$ compared to OH, indicating that first-stage ignition precedes other stages. Therefore, there are fundamentally different mechanisms that govern autoignition in both preheat cases.

To understand further the physics of autoignition at the different temperature conditions, conditional statistics are presented next. Figures 10 and 11 show conditional means of OH and $CH_3OCH_2O_2$, respectively, for the low-temperature case. In the figures, the different Reynolds numbers are compared at different times of the evolution of chemistry. Note that the OH conditional means at 0.18 s for Re = 10,000 is multiplied by 10^3 to fit into the same range as the other Reynolds numbers.

Consistently with the instantaneous profiles, peaks of OH and $CH_3OCH_2O_2$ coincide for the first 3 times shown. At the later time, $t = 0.18$ s, $CH_3OCH_2O_2$ is depleted relative to the earlier times while OH still exhibits higher peaks at leaner conditions corresponding

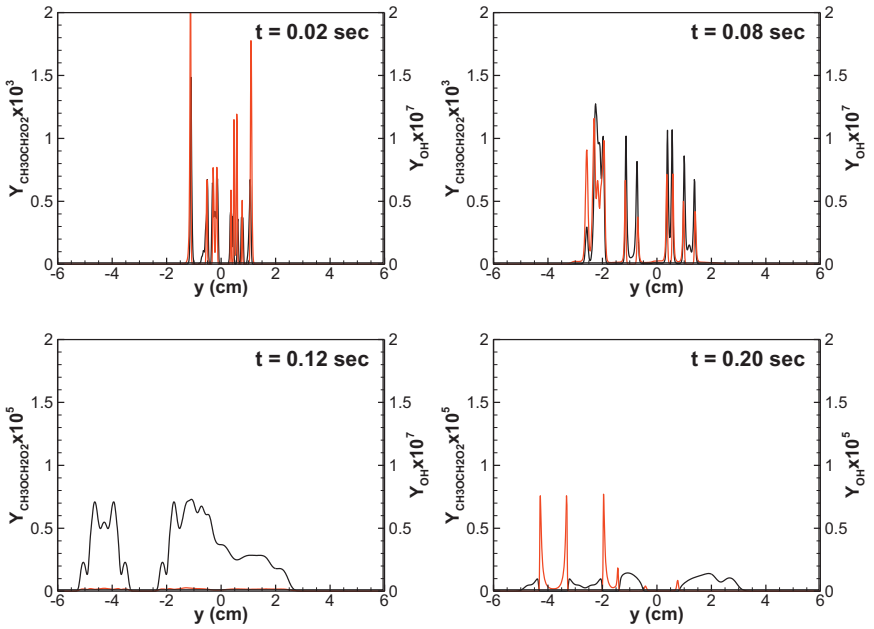

Fig. 8. Comparison of OH (red) and $CH_3OCH_2O_2$ (black) mass fraction profiles at different times for Re = 10,000 and the low-temperature case. (For interpretation of the references to color in this figure legend, the reader is referred to the web version of this article.)

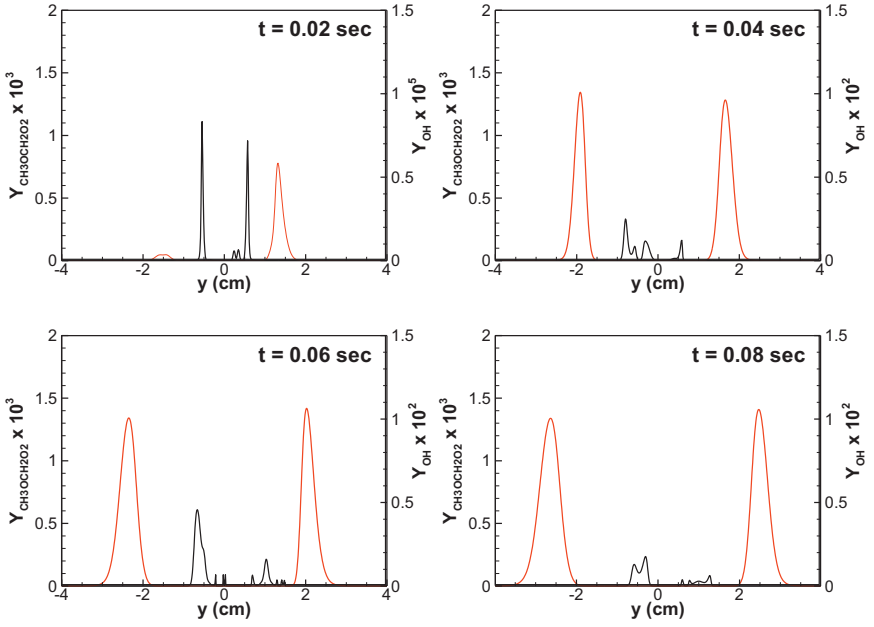

Fig. 9. Comparison of OH (red) and $CH_3OCH_2O_2$ (black) mass fraction profiles at different times for Re = 10,000 and the high-temperature case. Note that the scaling for different times are different for both species. (For interpretation of the references to color in this figure legend, the reader is referred to the web version of this article.)

to second stage ignition and consistently with the temperature conditional statistics (Fig. 6). At a later time, a second peak (not shown here) for OH at fuel-rich conditions (corresponding to the original peaks for first-stage ignition) is formed corresponding to second-stage ignition. As discussed earlier, second stage ignition at near-stoichiometric conditions occurs sooner for higher Reynolds numbers.

Figures 12 and 13 show conditional means of OH and $CH_3OCH_2O_2$, respectively, for the high-temperature case. In the figures, the different Reynolds numbers are compared at different times of the evolution of chemistry. In contrast to the low-temperature cases, the two sets of profiles in Figs. 12 and 13 show different patterns. First, the peaks of OH are present towards leaner conditions; while those of $CH_3OCH_2O_2$ are present at rich conditions. The autoignition process at values of mixture fractions from 0 to 0.2 appear to be governed primarily by high-temperature chemistry; while, at richer conditions, OH is barely present, but $CH_3OCH_2O_2$ indicate the presence of low-temperature chemistry for mixture fractions from 0.4 to 0.9 with a peak traveling towards richer conditions.

Understanding the interactions between the mixture fraction range 0–0.4 and those corresponding to higher mixture fractions

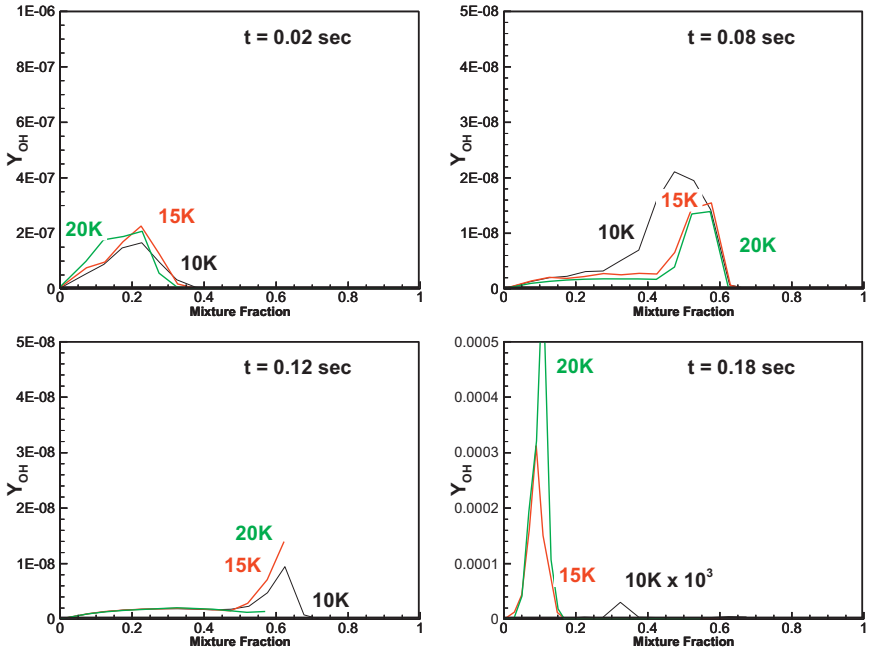

Fig. 10. Conditional means of OH mass fraction for Re = 10,000, 15,000 and 20,000 for the low-temperature conditions.

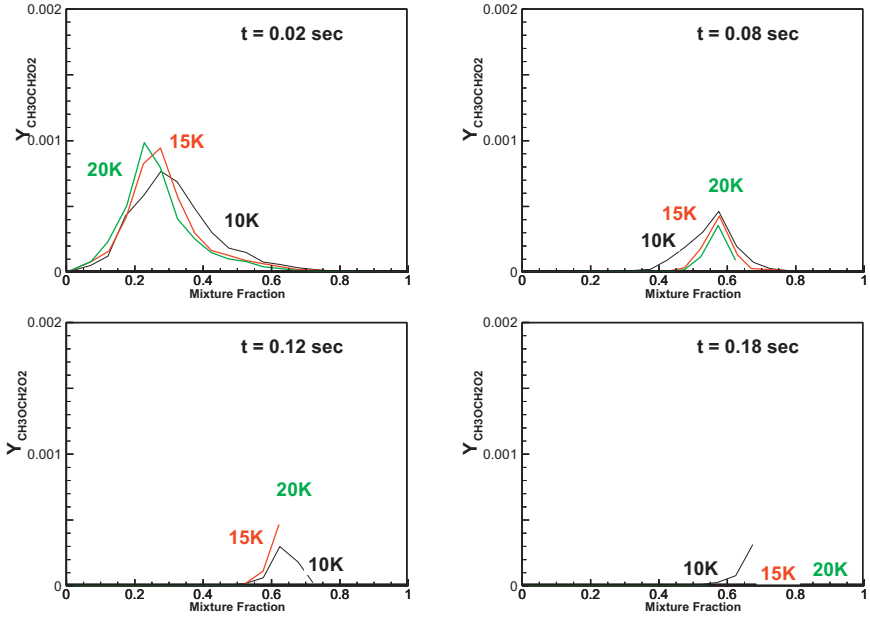

Fig. 11. Conditional means of $CH_3OCH_2O_2$ mass fraction for Re = 10,000, 15,000 and 20,000 for the low-temperature conditions.

can be better understood using conditional rms, which measure the magnitudes of fluctuations of the species. Figures 14 and 15 show conditional rms of OH and $CH_3OCH_2O_2$, respectively, for the low-temperature case corresponding to the same conditions as in Figs. 10 and 11. Here, and as expected, the peaks also coincide for the first 3 times, 0.02, 0.08 and 0.12 s, and indicate a migration of these peaks from leaner to richer fuel conditions. It is this process that can accelerate autoignition at cooler and richer fuel conditions.

Figures 16 and 17 show the same rms means for the high-temperature case. Again, two distinct behaviors for the two species are observed indicating the prevalence of single-stage ignition at leaner conditions.

4. Comparison of the homogeneous and jet configuration ignition scenarios

Having presented results of homogeneous and jet autoignition, an important question arises: can we anticipate potential scenarios of autoignition in non-homogeneous mixtures under turbulence conditions based on the homogeneous results alone? In the previous section, we have attempted to partially address this question by relating the observations for the jet configuration to those of 0D simulations. In the absence of turbulent and molecular transports, the various mixture conditions remain decoupled; while, we should expect a growing role of transport in accelerating or delaying ignition in the temporally-evolving jet configuration. Two

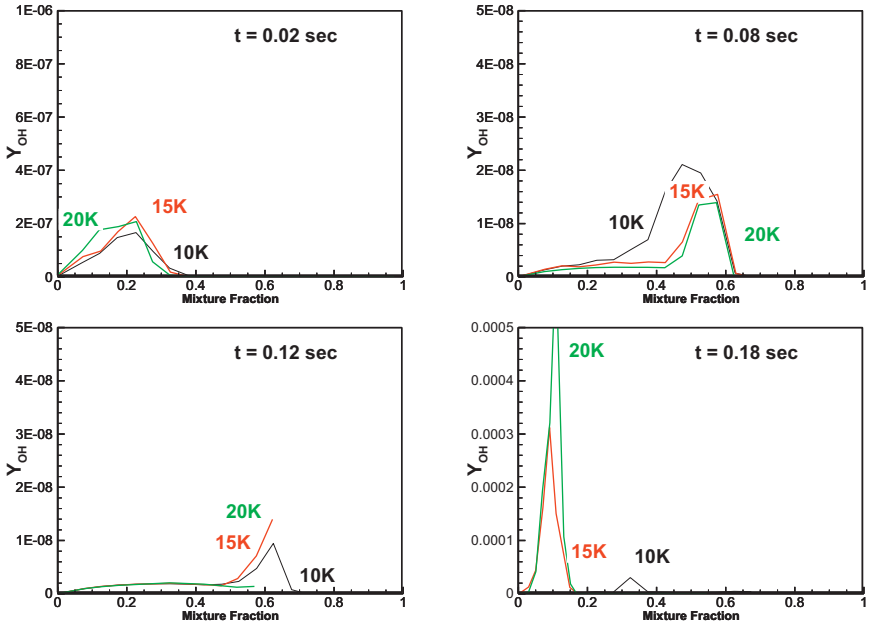

Fig. 12. Conditional means of OH mass fraction for Re = 10,000, 15,000 and 20,000 for the low-temperature conditions.

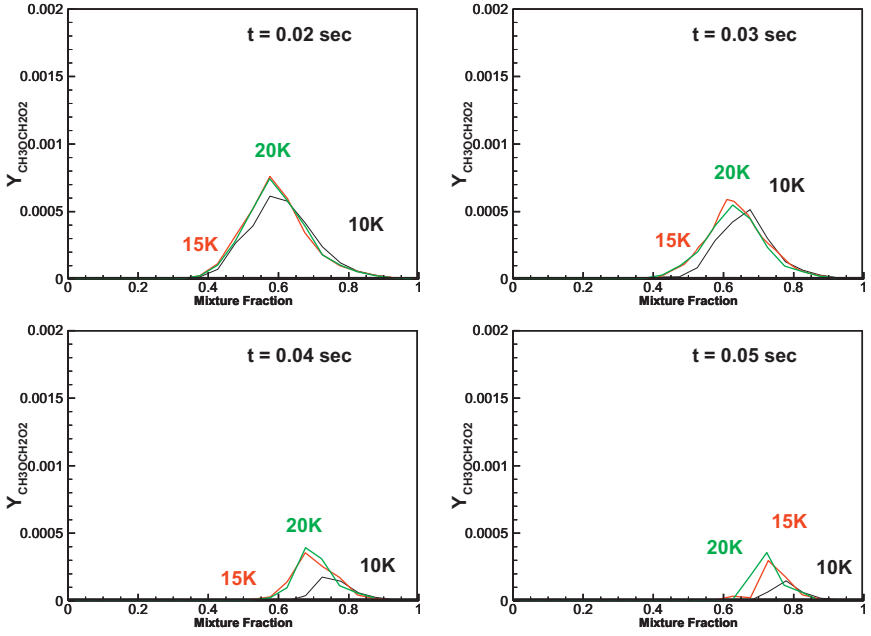

Fig. 13. Conditional means of $CH_3OCH_2O_2$ mass fraction for Re = 10,000, 15,000 and 20,000 for the high-temperature conditions.

important factors have been previously discussed by Echekki and Ahmed [14], which may be relevant here. First, the potential presence of a single-stage ignition process and a two-stage ignition process within mixtures can yield scenarios where the first stage of ignition in one mixture can serve to accelerate the process of single-stage ignition at a neighboring mixture. This scenario has occurred in the low-temperature simulations where the temperature rise started at lean conditions and 2-stage ignition occurred, then, further "propagated" towards richer conditions. Another scenario independent of this mechanism also occurred at conditions where the second ignition stage is lowest in the homogeneous mixture calculations.

The second factor is the shape of the ignition delay times (see Fig. 5) and whether it varies significantly as a function of mixture fraction. The presence of a strong variation enables an acceleration of ignition if the first factor is present, again, as observed in the low-temperature cases. Both factors resulted in the reduction of the autoignition delay as the Reynolds number is increased in contrast with the prevailing view of the role of turbulence in autoignition delay.

In contrast to the low-temperature scenario, the presence of a single-stage ignition process where ignition started in the higher-temperature scenarios, simply provided further mechanisms for the dissipation of heat and radicals (critical to the ignition process) by the combined effect of turbulence and molecular transport. This effect is even more pronounced in the range of mixture fractions between 0.4 and 0.6 (the cup-shaped region) where both first-stage and second-stage ignitions are present (see Fig. 5). Here, we believe that transport has thwarted the transition to the second stage of ignition.

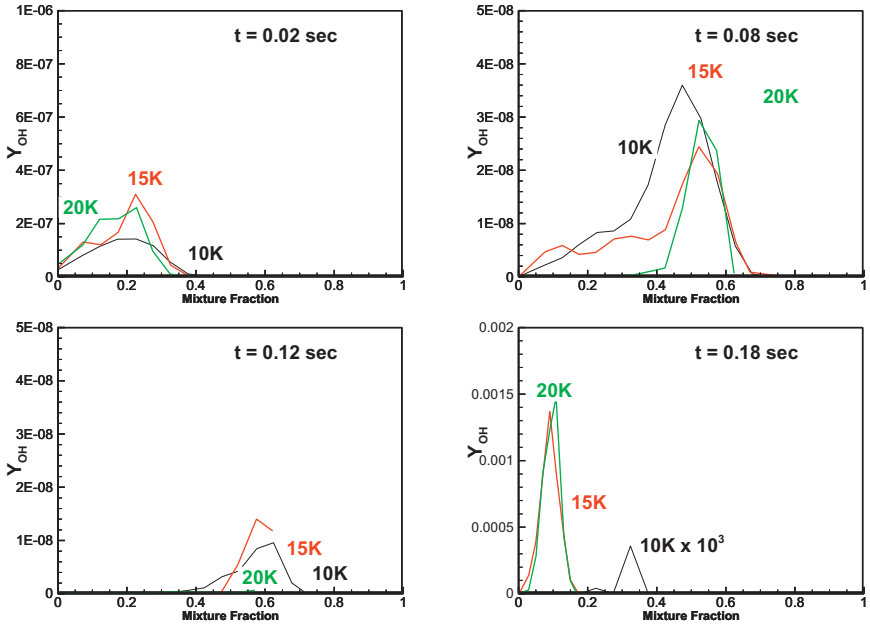

Fig. 14. OH mass fraction conditional rms at different times for Re = 10,000, 15,000 and 20,000 for the low-temperature conditions.

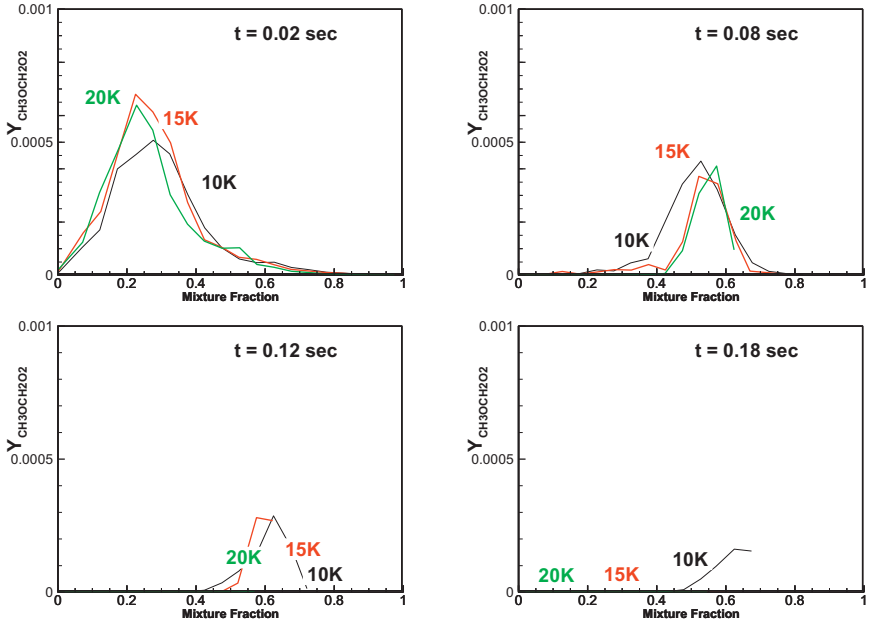

Fig. 15. $CH_3OCH_2O_2$ mass fraction conditional rms at different times for Re = 10,000, 15,000 and 20,000 for the low-temperature conditions.

Nonetheless, the scenarios established in both DME (i.e. this study) and n-heptane [14] autoignition and the additional scenarios established here, in particular the presence of a cup-shaped region in the statistics at mixture fractions between 0.4 and 0.6, appear to be "foretold" by the ignition delay maps under homogeneous mixtures regardless of the specific details of the reaction mechanisms of both fuels. This is an important observation that must be explored further with a broader range of fuels exhibiting NTC chemistry and a wider range of conditions to be considered.

5. Summary and conclusions

The autoignition of DME/air mixtures in a co-flow jet configuration with preheated air is investigated using the ODT model. Different inlet jet Reynolds numbers and two conditions for air preheat are considered. The simulations are carried out with a detailed chemical mechanism for DME oxidation. These simulations were augmented with homogeneous mixtures' simulations at different mixture conditions consistent with the preheated air and fuel references states.

The simulations show that turbulence plays different and potentially competing roles for this fuel, which can be subject to NTC effects. The first role is that scalar dissipation tends to delay ignition due to heat and radical losses from nascent kernels. This trend is observed at the high-temperature conditions where ignition starts in a single-stage ignition regime. It also contributes to important reduction in the ignition delay time at lower temperatures where ignition starts in the first stage of a two-stage ignition, which serves to ignite neighboring layers of the mixture.

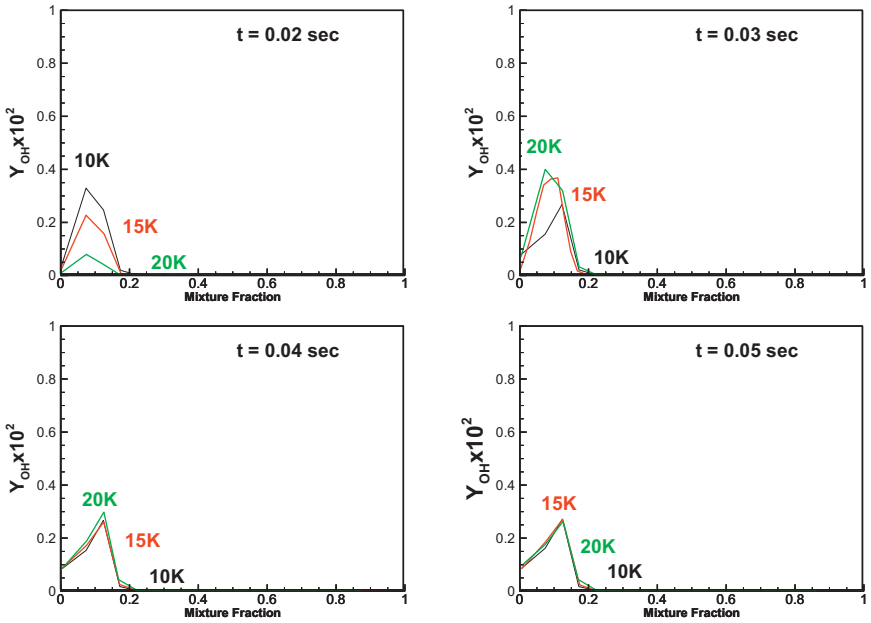

Fig. 16. OH mass fraction conditional rms at different times for Re = 10,000, 15,000 and 20,000 for the high-temperature conditions.

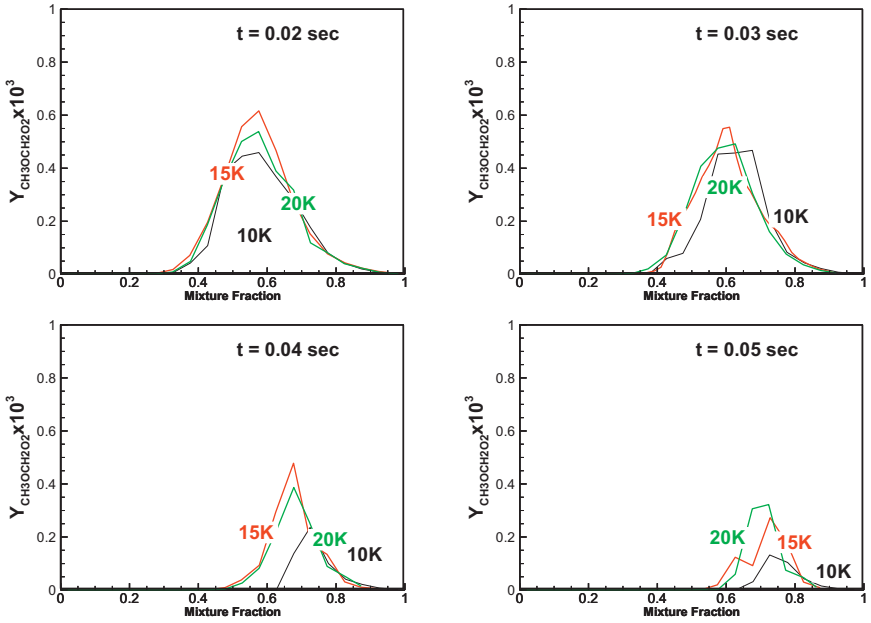

Fig. 17. $CH_3OCH_2O_2$ mass fraction conditional rms at different times for Re = 10,000, 15,000 and 20,000 for the high-temperature conditions.

By comparing our present results to our previous study on n-heptane autoignition in a similar geometry [14], we find that ignition delay maps as functions of mixture fraction can provide important insight into the mechanisms by which transport can accelerate or delay autoignition beyond additional considerations of the specific details of the autoignition chemistry of the fuel.

Acknowledgments

This paper was made possible by an NPRP award [NPRP 6-105-2-039] from the Qatar National Research Fund (a member of The Qatar Foundation). The statements made here are solely the responsibility of the authors. S.F. Ahmed would like to thank Qatar University for the support.

References

[1] E. Mastorakos, T.A. Baritaud, T.J. Poinsot, Numerical simulations of autoignition in turbulent mixing flows, Combust. Flame 109 (1997) 198–223.
[2] C.N. Markides, E. Mastorakos, An experimental study of hydrogen autoignition in a turbulent co-flow of heated air, Proc. Combust. Inst. 30 (2005) 883–891.
[3] C.N. Markides, G. De Paola, E. Mastorakos, Measurements and simulations of mixing and autoignition of an n-heptane plume in a turbulent flow of heat air, Exp. Thermal Fluid Sci. 31 (2007) 293–401.
[4] T. Echekki, K. Gupta, Hydrogen autoigniiton in a turbulent jet with preheated co-flow air, Int. J. Hydrogen Energy 34 (2009) 8352–8377.
[5] K. Gupta, T. Echekki, One-dimensional turbulence model simulations of autoignition of hydrogen/carbon monoxide fuel mixtures in a turbulent jet, Combust. Flame 158 (2011) 327–344.
[6] H.G. Im, J.H. Chen, C.K. Law, Ignition of hydrogen–air mixing layer in turbulent flows, Symp. (Int.) Combust. 27 (1998) 1047–1056.
[7] R. Hilbert, D. Thévenin, Autoignition of turbulent non-premixed flames investigated using direct numerical simulations, Combust. Flame 128 (2002) 22–37.

[8] T. Echekki, J.H. Chen, Direct numerical simulation of autoignition in non-homogeneous hydrogen–air mixtures, Combust. Flame 134 (2003) 169–191.
[9] P.R. Medwell, P.A.M. Kalt, B.B. Dally, Simultaneous imaging of OH, formaldehyde and temperature of turbulent nonpremixed jet flames in a heated and diluted coflow, Combust. Flame 148 (2007) 48–61.
[10] E. Oldenhof, M.J. Tummers, E.H. van Veen, D.J.E.M. Roekaerts, Role of entrainment in the stabilization of jet in jet-in-hot-coflow flames, Combust. Flame 158 (2011) 1553–1563.
[11] S. Deng, P. Zhao, D.L. Zhu, C.K. Law, NTC-affectd ignition and low-temperature flames in nonpremixed DME/air counterflow, Combust. Flame 161 (2014) 1993–1997.
[12] G. Bansal, A. Mascarenhas, J.H. Chen, Direct numerical simulations of autoignition in stratified dimethyl-ether (DME)/air turbulent mixtures, Combust. Flame 162 (2015) 688–702.
[13] H.A. El-Asrag, Y. Ju, Direct numerical simulations of NOx effect on multistage autoignition of DME/air mixture in the negative temperature coefficient regime for stratified HCCI engine conditions, Combust. Flame 161 (2014) 256–269.
[14] T. Echekki, S.F. Ahmed, Autoignition of n-heptane in a turbulent co-flowing jet, Combust. Flame 162 (2015) 3829–3846.
[15] T. Echekki, A.R. Kerstein, T.D. Dreeben, J.-Y. Chen, 'One-dimensional turbulence' simulation of turbulent jet diffusion flames: model formulation and illustrative applications, Combust. Flame 125 (2001) 1083–1105.
[16] S. Deng, P. Zhao, M.E. Mueller, C.K. Law, Autoignition-affected stabilization of laminar nonpremixed DME/air coflow flames, Combust. Flame 162 (2015) 3437–3445.
[17] S. Deng, P. Zhao, M.E. Mueller, C.K. Law, Stabilization of laminar nonpremixed DME/air coflow flames at elevated temperatures and pressures, Combust. Flame 162 (2015) 4471–4478.
[18] S. Deng, P. Zhao, M.E. Mueller, C.K. Law, Flame dynamics in oscillating flows under autoignitive conditions, Combust. Flame 168 (2016) 75–82.
[19] Y. Minamoto, J.H. Chen, DNS of a turbulent lifted DME jet flame, Combust. Flame 169 (2016) 38–50.
[20] P. Zhao, M. Chaos, A. Kazakov, F.L. Dryer, Thermal decomposition reaction and a comprehensive kinetic model of dimethyl ether, Int. J. Chem. Kinet. 40 (2008) 1–18.
[21] P. Dagaut, J.C. Boettner, M. Cathonnet, Chemical kinetic study of dimethyl ether oxidation in jet stirred reactor from 1 to 10 atm: experiments and kinetic modeling, Symp. (Int.) Combust. 26 (1996) 627–632.
[22] H.J. Curran, W.J. Pitz, C.K. Westbrook, P. Dagaut, J.C. Boettner, M. Cathonnet, A wide range modeling study of dimethyl ether oxidation, Int. J. Chem. Kinet. 30 (1998) 229–241.
[23] P. Dagaut, C. Daly, J.M. Simmie, M. Cathonnet, The oxidation and ignition of dimethyl ether in a jet-stirred reactor, Symp. (Int.) Combust. 27 (1998) 361–369.
[24] S.L. Fischer, F.L. Dryer, H.J. Curran, The reaction kinetics of dimethyl ether. I: high-temperature pyrolysis and oxidation in flow reactors, Int. J. Chem. Kinet. 32 (2000) 713–740.
[25] H.J. Curran, S.L. Fischer, F.L. Dryer, The reaction kinetics of dimethyl ether. II: low-temperature oxidation in flow reactors, Int. J. Chem. Kinet. 32 (2000) 741–759.
[26] E.W. Kaiser, T.J. Wallington, M.D. Hurley, J. Platz, H.J. Curran, W.J. Pitz, Westbrook C.K., Experimental and modeling study of premixed atmospheric-pressure dimethyl ether–air flames, J. Phys. Chem. A 104 (2000) 8194–8206.
[27] A.E. Lutz, R.J. Kee, J.A. Miller, SENKIN: A Fortran program for predicting homogeneous gas phase chemical kinetics with sensitivity analysis, Sandia National Laboratories, Livermore, CA, USA, 1988 Report 87-8248.
[28] J.C. Hewson, A.R. Kerstein, Stochastic simulation of transport and chemical kinetics in turbulent $CO/H_2/N_2$ flames, Combust. Theory Model. 5 (2001) 669–697.
[29] J.C. Hewson, A.R. Kerstein, Local extinction and reignition in nonpremixed turbulent $CO/H_2/N_2$ jet flames, Combust. Sci. Technol. 174 (2002) 35–66.
[30] S. Zhang, T. Echekki, Stochastic modeling of finite-rate chemistry effects in hydrogen–air turbulent jet diffusion flames with helium dilution, Int. J. Hydrogen Energy 33 (2008) 7295–7306.
[31] B. Ranganath, T. Echekki, One-dimensional turbulence-based closure for turbulent non-premixed flames, Prog. Comput. Fluid Dyn. 6 (2006) 409–418.
[32] B. Ranganath, T. Echekki, ODT-closure with extinction and reignition in piloted methane-air jet diffusion flames, Combust. Sci. Technol. 181 (2009) 597–617.
[33] P.N. Brown, G.D. Byrne, A.C. Hindmarsh, VODE: A variable-coefficient ODE solver, SIAM J. Sci. Stat. Comput. 10 (1989) 1038–1051.
[34] R.J. Kee, J. Warnatz, J.A. Miller, Fortran computer-code package for the evaluation of gas-phase viscosities, conductivities, and diffusion coefficients, Sandia National Laboratories, Livermore, CA, USA, 1983 Report No. SAND 83-8209.
[35] R.J. Kee, J.A. Miller, T.H. Jefferson, Chemkin: A general-purpose, problem-independent, transportable, Fortran chemical kinetics code package, Sandia National Laboratories, Livermore, CA, USA, 1980 Report SAND80-8003.
[36] R.W. Bilger, The structure of turbulent nonpremixed flames, Symp. (Int.) Combust. 22 (1988) 475–488.
[37] A. Krisman, E.R. Hawkes, M. Talei, A. Bhagatwala, J.H. Chen, Polybrachial structures in dimethyl ether edge-flames at negative temperature coefficient conditions, Proc. Combust. Inst. 35 (2015) 999–1006.